JOURNAL OF THERMOPHYSICS AND HEAT TRANSFER
Vol. 10, No. 1, January–March 1996

Thermodynamic Charts for Nonequilibrium Plasma Flow in a Supersonic Nozzle

Kuan Chen*
University of Utah, Salt Lake City, Utah 84112
and
Thomas L. Eddy†
EG&G Idaho, Idaho Falls, Idaho 83415

Presented in this article is a one-dimensional, nonequilibrium analysis for reacting flow in a supersonic nozzle. Thermodynamic charts of different entropy values were developed to take into account the effects of finite reaction rate during the transition from local chemical equilibrium (LChE) to frozen flow. At a given entropy the LChE curve was calculated first. Frozen flow solutions starting at different points on the LChE curve were then computed and plotted on a constant-entropy plane. The first and second laws of thermodynamics were employed to determine the ranges of valid solutions on different constant-entropy planes. Variations of temperature, pressure, and chemical affinity along the nozzle were computed for argon plasma at 10 atm and 15,000 K discharged through a supersonic nozzle to 0.05 atm. Effects of entropy change on the region of valid plasma states that were bounded by LChE and frozen flow solutions were examined. Three-dimensional plots were made to assist in viewing the variations of plasma state and nozzle performance when irreversibility due to finite reaction rates was considered. It was found that the range of valid states for a reacting flow decreases as entropy increases. Consequently, only charts within a certain entropy range are needed for a given reservoir condition.

Nomenclature

A = flow cross-sectional area
e^- = free electron
F = chemical affinity
g_m = degeneracy of energy level m
H^0 = negative value of the heat of reaction
h = enthalpy
$\underline{h}$ = Planck's constant
K_p = equilibrium constant
k = Boltzmann's constant
M = chemical symbol for reactants and products
m = mass
N = particle number
n = number density
p = pressure
s = entropy
T = temperature
V = volume
v = velocity
w = reaction rate
X = mole fraction
x = distance from the nozzle inlet
Z = partition function
Δh = enthalpy of formation
ε_m = energy of level m referred to the ground state
μ = chemical potential
ν = stoichiometric coefficient
ρ = density
ω = forward reaction rate

Subscripts
chem = chemical energy
e = evaluated at the nozzle exit
f = evaluated at the point in the LChE curve where frozen flow begins
j = species j
m = energy level
p = products of chemical reaction
r = reactants of chemical reaction
t = translational energy mode
x = electronic excitation energy mode
0 = evaluated at the reservoir state

Superscripts
0 = refers to reference pressure
* = dimensionless quantities

I. Introduction

IT is common knowledge to researchers in the gasdynamics area that high-speed, high-temperature gas flows such as those encountered in advanced propulsion systems are not in local thermodynamic equilibrium (LTE) and nonequilibrium flow analysis should be employed for composition and property calculations. The flowfield in the analysis of a supersonic nozzle flow is generally divided into three regions[1]: 1) an equilibrium flow in the converging portion and the throat of the nozzle due to the relatively low flow velocities and high pressures, 2) a frozen flow region far downstream of the diverging section in which the composition is invariant, and 3) a region downstream of the throat where chemical nonequilibrium exists. Flows in these regions should be treated separately.

Most of recent studies of supersonic nozzle flow solved the chemical rate equations in the chemical nonequilibrium region. However, the accuracy of reaction equation calculations is often questionable and in some cases calculations may fail to converge when plasma flows are involved in high-speed nozzle flows. The difficulties and uncertainty in the determination of plasma reaction rates were discussed and demon-

Presented as Paper 94-2414 at the AIAA 25th Plasmadynamics and Laser Conference, Colorado Springs, CO, June 20–23, 1994; received Dec. 5, 1994; revision received June 16, 1995; accepted for publication July 17, 1995.

*Associate Professor, Mechanical Engineering Department.
†Principal Engineer, Idaho National Engineering Laboratory.

strated in many plasma texts and papers.[2-4] Phelps computed the collision cross sections of hydrogen plasma.[3] Ionization and recombination rate coefficients for argon plasma at moderate-to-high ionization degree can be found in the book by Lelevkin et al.[4] Generally, rate coefficients for ionization and recombination of plasmas are deduced from elaborate collisional–radiative models. On the other hand, it is relatively simple and less time consuming to compute the composition and properties of frozen flows and flows in local chemical equilibrium (LChE). Since the state of a reacting flow with finite reaction rate should be bounded by the states of frozen (zero reaction rate) and LChE flows (infinite reaction rate), studying these two limiting cases of flow would be helpful to understanding the real flow situation and estimating the ranges of composition and property variations when accurate reaction rate data are unavailable and/or when the stiff reaction equations are difficult to solve.

Frozen and LChE flow solutions for supersonic nozzle analysis can be found in many gasdynamics textbooks.[5,6] Most of these previous analyses computed the frozen flow with composition identical to that of the reservoir state and the LChE flow at one entropy value, and assumed that all of the intermediate-rate solutions fall between the results of these two flows. LChE or frozen flows are isentropic if one assumes the nozzle is adiabatic and the flows are inviscid.[5] The two curves and all of the states in between on the constant-entropy plane have the same entropy value as the gas in the reservoir. Chemical reactions with finite reaction rates are irreversible processes and the gas entropy should increase; therefore, the state of a nonequilibrium flow with finite reaction rate may fall outside the bounds of the LChE and frozen flow solutions calculated at the reservoir entropy as exemplified by Anderson.[5]

Presented in this article is a one-dimensional thermodynamic analysis for developing nonequilibrium charts applicable to reacting plasma flows. The range of possible entropy values for a given reservoir state was investigated. Charts of different entropy values were constructed to study the effects of finite reaction rate during transition from LChE to frozen flow. The momentum and energy equations at a given entropy value were solved by iteration. Variations of thermodynamic properties for argon plasma through a supersonic nozzle were computed for a reservoir state of 10 atm and 15,000 K. Relations between entropy change and the valid values of temperature, pressure, and affinity variations were examined.

It was found that when the first and second laws of thermodynamics were both taken into consideration, the region of plasma states bounded by the LChE and frozen flow solutions on a constant-entropy plane shrank very rapidly as entropy increased from the reservoir state. Thus, for a given reservoir state, only charts within a certain entropy range are needed for nozzle flow analysis. If an area-pressure-entropy diagram is employed to define the region of valid states, the range of plasma states at high entropies may fall outside the bounds of valid plasma states on the minimum entropy plane. If affinity instead of the flow cross-sectional area is used, the region of valid states at high entropy values will fall within the valid state envelope calculated at the reservoir entropy. This result suggests that affinity is convenient to use in the analysis of reacting flows through nozzles.

II. Construction of Nonequilibrium Charts for Nozzle Flows

Shown in Fig. 1 is an ionized gas or gas mixture discharged through a supersonic nozzle. If one-dimensional analysis is employed, the thermodynamic and flow properties of the plasma can be expressed as functions of x or A of the nozzle. The chemical composition of a reacting flow may also vary with x or A. The state of a reacting flow at a given x or A depends not only on the upstream conditions, but also on the nozzle

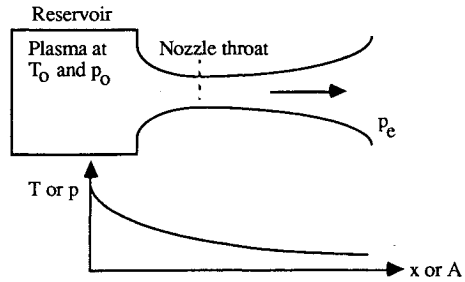

Fig. 1 One-dimensional plasma flow in an adiabatic supersonic nozzle.

angle. The flow with a smaller nozzle angle is more likely to be in LChE than a flow with a larger nozzle angle at the same A, since the time required for the gas to travel between two areas is longer, allowing more collisions to occur. Thus, the gas state at a given cross section may vary from the LChE state (corresponding to an infinitely fast reaction rate or an infinitesimally small nozzle angle) to the frozen flow result (corresponding to a zero reaction rate or an infinitely large nozzle angle). Measuring T and p is not sufficient to define the state of a reacting flow. The degree of reaction extent must also be specified.

Chemical affinity is used in nonequilibrium thermodynamic processes as a measure of the degree of reaction extent.[7,8] For an elementary reaction

$$\sum \nu_r(M_r) \leftrightarrow \sum \nu_p(M_p) \tag{1}$$

the affinity of the reaction is defined as

$$F = -\sum \nu_j \mu_j \tag{2}$$

The affinity of the previous reaction for a gas in local thermal equilibrium (LThE) is related to the reaction rate by the following equation[8]:

$$w = \omega\{1 - \exp[-F/(kT)]\} \tag{3}$$

Affinity is a thermodynamic property (a point function). Change in affinity depends on the state of the system and is independent of the path by which the system arrived at the given state. Thermodynamic tables or charts can be constructed at different affinity values for the calculations of properties and compositions of plasma flows not in chemical equilibrium.[9,10]

Since all reactions with finite reaction rates must fall between the states of infinite and zero reaction rates, calculation of LChE and frozen flows enables us to estimate the ranges of gas properties and nozzle performance at a given A. However, the region bounded by the LChE curve and the curve of flow frozen at the reservoir pressure ($p_f = p_0$) on a constant-entropy plane is the family of frozen flow solutions of different frozen point pressures (at $p_f \leq p_0$). The states of finite reaction rates do not lie in this plane because the entropy is increased. On a plane of constant entropy, a point on the LChE curve is also a frozen flow solution starting at that point, providing that transition from LChE to frozen flow can take place without entropy change. This implies that the nozzle angle changes abruptly from zero to infinite and the flow can follow the nozzle contour perfectly. In practice, this kind of nozzle flow is impossible. Transition from LChE to frozen flow in nozzle operation cannot occur on a plane of constant entropy. The change of state of an inviscid reacting flow is depicted in the three-dimensional plot of Fig. 2. If the flow speed is low and pressure is high from state a to state b, the state of the gas flow should follow the LChE curve on the plane of $s = s_0$ until point b is reached. Transition from LChE to frozen flow takes place from b to d, causing the state of

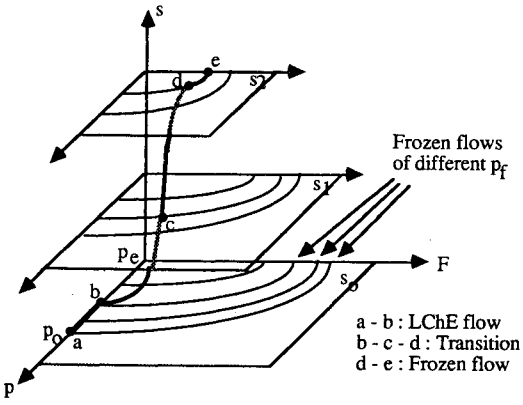

Fig. 2 Transition from LChE to frozen flow.

the gas to leave the plane of $s = s_0$ and reach a higher entropy value $s = s_2$. After point d, the state of the gas will follow the frozen flow line that passes through point d on the plane of $s = s_2$ until the exit state e is reached. Figure 2 clearly illustrates that nonequilibrium charts of different entropy values are needed for the analysis of transition between LChE and frozen flows in a reacting flow.

The development and application of nonequilibrium charts for reacting flow analyses can be better understood with the aid of an example. Let us consider argon plasma at 15,000 K and 10 atm discharged through a supersonic nozzle to an exit pressure of 0.05 atm. The flow is assumed to be one dimensional, inviscid, and adiabatic. For temperatures below 20,000 K, the dominant ionization reaction is expected to be the formation of the singly ionized argon ions:

$$\mathrm{Ar} \leftrightarrow \mathrm{Ar}^+ + \mathrm{e}^- \tag{4}$$

As a result, only the recombination of argon atoms from singly ionized argon ions and electrons is considered in the present analysis. The range of affinity variation can be plotted as a function of p on the plane of constant entropy for a given entropy value, as depicted in Fig. 2. If more than one chemical reaction is equally important, affinities associated with all important reactions should be utilized to define the plasma state. In this case, construction of the affinity charts is more involved.

At low temperatures, only the first few electronic levels are important to equilibrium constant and property calculations. The electronic levels employed in the present calculation of argon composition and properties are those used in Sonntag and Van Wylen's book[11] for argon plasma around 10,000 K. At high temperatures, ionization of other argon ions such as Ar^{++} and Ar^{+++} should be taken into consideration and a large number of electronic energy levels should be included. Sedghinasab and Eddy's calculation[12] of argon properties included the first four argon ions and for electronic energy levels of up to 70. The good agreement between the present calculation and Sedghinasab and Eddy's results of LTE argon properties justifies the assumptions of one dominant ionization–recombination reaction and negligible high electronic energy levels for the temperature range considered here.

For a gas mixture not in local chemical equilibrium, the properties and composition are functions of pressure, temperature(s), and chemical affinity. For the simple recombination reaction of argon plasma:

$$\mathrm{Ar}^+ + \mathrm{e}^- \rightarrow \mathrm{Ar} \tag{5}$$

the partial pressures can be determined from[13]

$$(p_{\mathrm{Ar}}/p^0)/[(p_{\mathrm{e}^-}/p^0)(p_{\mathrm{Ar}^+}/p^0)] = \exp[F/(kT)]/K_p \tag{6}$$

$$p_{\mathrm{Ar}} = p - p_{\mathrm{e}^-} - p_{\mathrm{Ar}^+} = p - 2p_{\mathrm{e}^-} \tag{7}$$

where p_j is the partial pressure of species j, F is the affinity, and K_p the equilibrium constant at temperature T evaluated at a reference pressure p^0. The mole fraction of the free electrons in the mixture at p can be determined from

$$(1 - 2X_{\mathrm{e}^-})/X_{\mathrm{e}^-}^2 = (p^0/p)\exp[F/(kT)]/K_p \tag{8}$$

where

$$X_{\mathrm{e}^-} = p_{\mathrm{e}^-}/p = n_{\mathrm{e}^-}/n \tag{9}$$

With the chemical composition determined from the previous equations, the density and specific enthalpy of argon plasma can be calculated from

$$\rho = \sum m_j n_j \tag{10}$$

$$h = \sum m_j n_j h_j \tag{11}$$

where

$$h_j = h_{t,j} + h_{x,j} + h_{\mathrm{chem},j} \tag{12}$$

$$h_{t,j} = 2.5kT_{t,j} \tag{13}$$

$$h_{x,j} = kT_{x,j}Z'_{x,j}/Z_{x,j} \tag{14}$$

$$Z_{x,j} = \sum g_{xm} \exp[-\varepsilon_{xm}/(kT_{x,j})] \tag{15}$$

$$Z'_{x,j} = \sum g_{xm}[\varepsilon_{xm}/(kT_{x,j})]\exp[-\varepsilon_{xm}/(kT_{x,j})] \tag{16}$$

$$h_{\mathrm{chem},j} = 0 \quad \text{for } j = \mathrm{Ar} \text{ and } \mathrm{e}^-$$

$$h_{\mathrm{chem},j} = 2.5264 \times 10^{-9} \text{ erg} = 2.5264 \times 10^{-19} \text{ kJ} \quad \text{for } j = \mathrm{Ar}^+ \tag{17}$$

The entropy of the argon plasma is calculated from

$$s = \sum m_j n_j s_j \tag{18}$$

where

$$s_j = s_{t,j} + s_{x,j} \tag{19}$$

$$s_{t,j} = k[\mathscr{N}(Z_{t,j}/N_j) + 2.5] \tag{20}$$

$$s_{x,j} = k(\mathscr{N} Z_{x,j} + Z'_{x,j}/Z_{x,j}) \tag{21}$$

$$Z_{t,j}/N_j = (2\pi m_j/\underline{h}^2)^{3/2}(kT_{t,j})^{5/2}/p_j \tag{22}$$

$$T_{t,j} = T_{x,j} = T \text{ for a LThE gas} \tag{23}$$

Computation of reacting flow properties at a given entropy value started with the construction of the LChE curve. A plasma pressure $p < p_0$ was selected and the corresponding T was guessed. X_j and n_j were then calculated from Eqs. (8) and (9) and the ideal gas law. With number densities n_j determined, ρ, h, and s can be computed from Eqs. (10) to (18). Iteration on T continued until the calculated s was very close to the given s value. p was then changed to a smaller value and the computation of LChE properties repeated until the exit pressure was reached.

After the LChE curve was constructed, frozen flow curves starting at different points on the LChE curve were calculated. The procedure for computing the frozen flow solutions was similar to that for the LChE curve, except that mole fractions X_j were determined from the LChE state at which frozen flow started. Equation (8) was not used for composition calculation

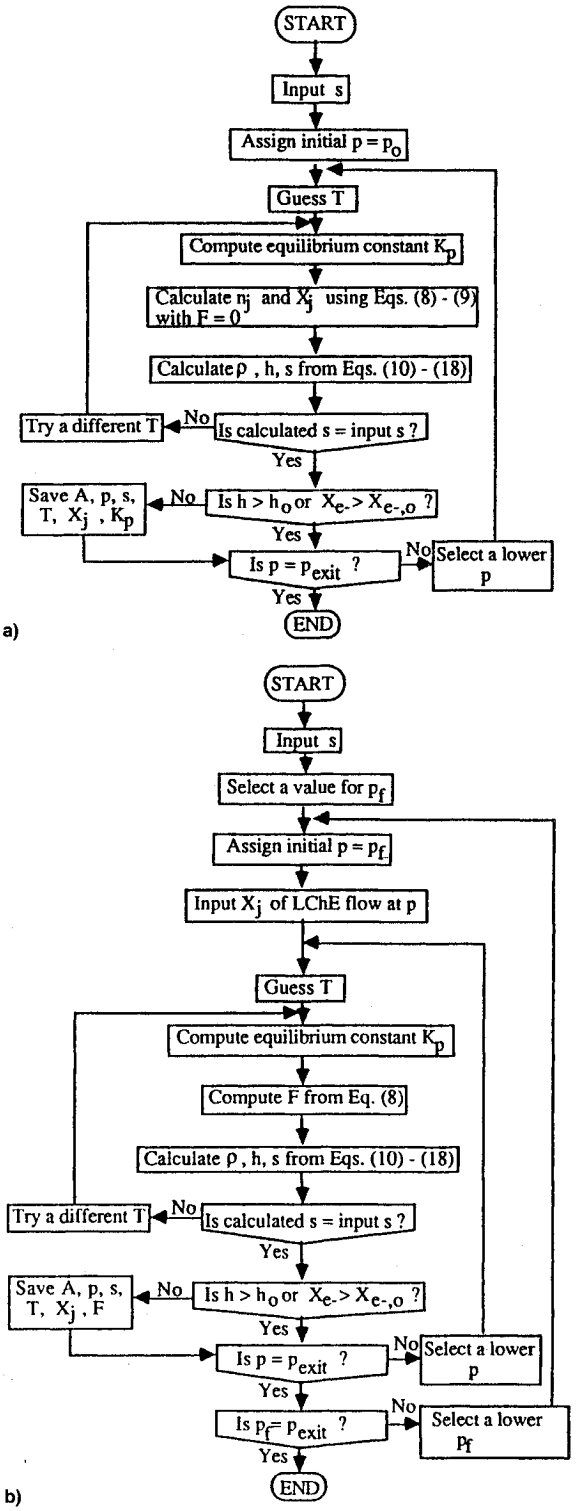

Fig. 3 Flow charts for LChE and frozen flow calculations: a) LChE curve and b) frozen flows.

of frozen flows. It was used to determine F of a frozen flow at a given T and p. The flow charts of the solution algorithms for LChE and frozen flows are shown in Figs. 3a and 3b.

Flow properties were calculated from the conservation principles of mass and energy after the thermodynamic properties were determined. For a one-dimensional, steady adiabatic flow from state 1 to state 2 with negligible potential energy change, the first law of thermodynamics becomes

$$h_2 = h_1 + (v_2^2 - v_1^2)/2 \tag{24}$$

The flow cross-sectional area can be determined from the previous equation and the conservation of mass requirement:

$$\rho v A = \text{const} \tag{25}$$

Since the nozzle throat area for a given reservoir condition changes with reaction extent, it is not appropriate to use the nozzle throat area for normalizing the flow cross-sectional area. The area calculated in the present analysis is the area required for a unit mass flow rate $\rho v A = 1$ kg/s. The charts generated in this article can be used to analyze other one-dimensional flows with mass flow rates different than 1 kg/s if the values of A in the charts are changed proportionally. (For instance, if the mass flow rate were changed from 1 to 2 kg/s, the values of A in Figs. 5 and 6 should be doubled.)

III. Results and Discussion

The valid ranges of several thermodynamic and flow properties for argon plasma at 10 atm and 15,000 K discharged through an adiabatic, frictionless nozzle were calculated and studied. Among the various thermodynamic properties of a reacting flow, entropy, and affinity are most useful to nozzle efficiency and performance analysis. Increase in entropy in an adiabatic flow is directly related to the loss of high-grade energy such as the product of thrust and distance (which is the work done by a rocket). Affinity is a measure of the degree of reaction extent. A zero affinity indicates the completion of chemical reaction and that all chemical energy is released in a recombination reaction. High affinity values imply low degrees of recombination reaction and a large quantity of chemical energy is still frozen in the plasma flow. Zero affinity and minimum entropy increase are desired for maximum thrust in nozzle operation. In addition to the entropy and affinity charts, the ranges of valid pressures and temperatures were also plotted for discussion since these two properties are directly measurable and commonly used in nozzle analyses.

In the preparation of the nonequilibrium charts, it was postulated that the argon plasma in the reservoir was in local chemical equilibrium. The LChE calculation at the reservoir pressure and temperature yielded

$$h_0 = 18{,}093 \text{ kJ/kg} \tag{26}$$

$$s_0 = 6.213 \text{ kJ/kg-K} \tag{27}$$

$$X_{e^-,0} = p_{e^-,0}/p_0 = 0.182 \tag{28}$$

In an adiabatic flow of the recombination of argon plasma, h can never be higher than h_0 and s must be higher than or equal to s_0. In addition, X_{e^-} should be less than $X_{e^-,0}$. These constraints limit the range of possible plasma states in the

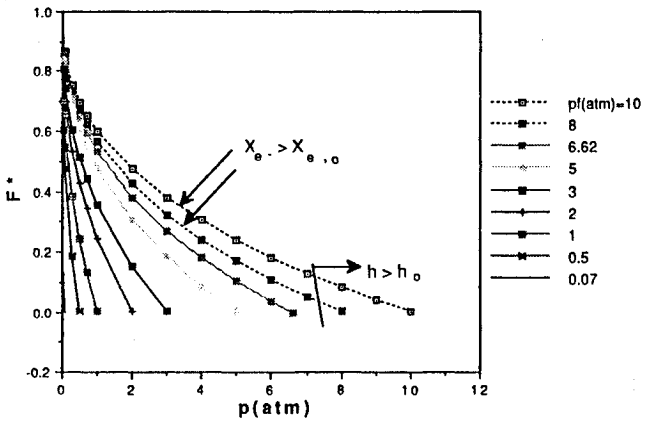

Fig. 4 Pressure-affinity diagram of valid argon states at s = 6.3 kJ/kg-K.

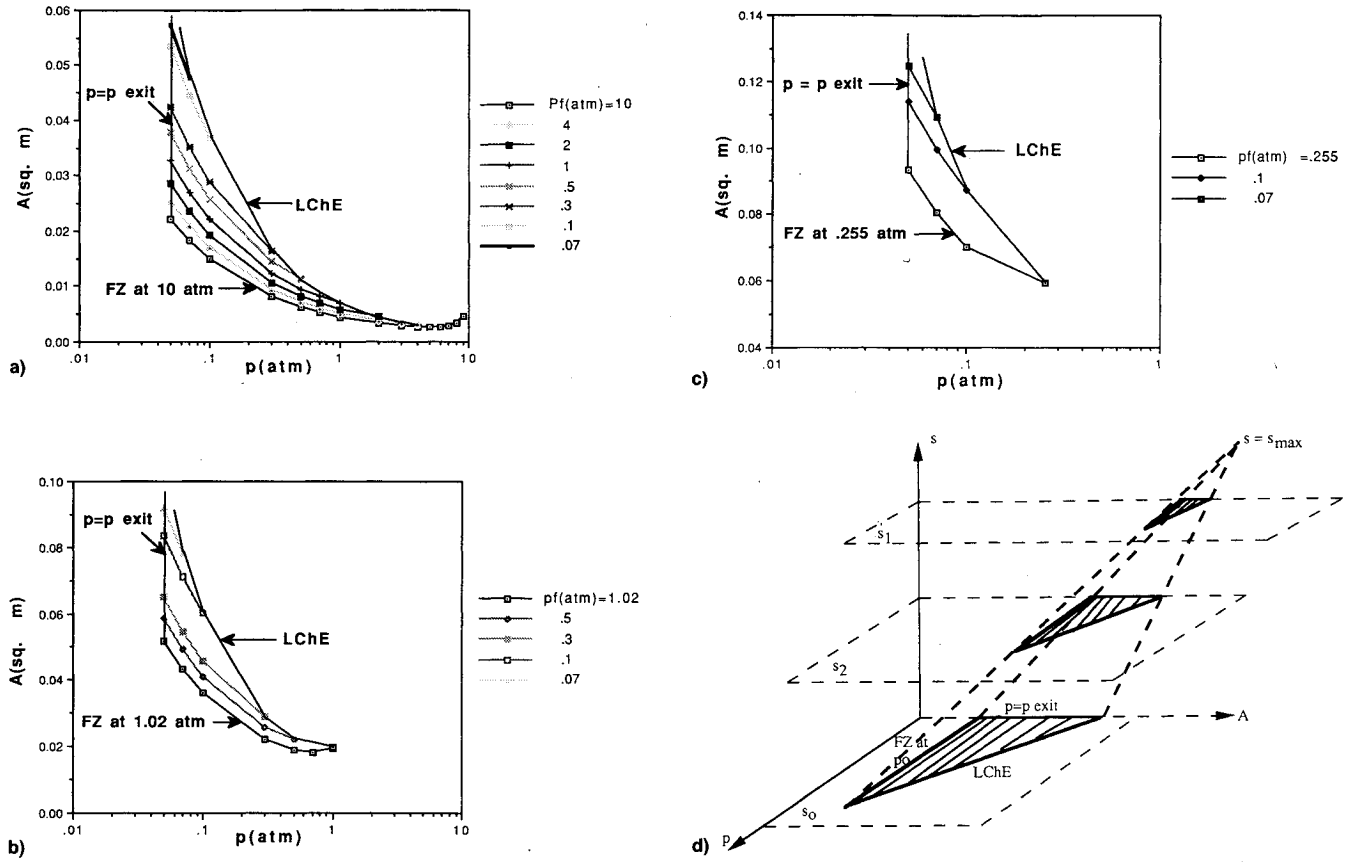

Fig. 5 Pressure-area diagrams of valid argon states at different entropies. s = a) 6.213 ($=s_0$), b) 6.7, c) 7, and d) 6.213–7 kJ/kg-K.

nonequilibrium charts. At a given pressure, both h and X_{e^-} increase as s increases. Thus at high s, only plasmas frozen at low pressures satisfy the requirements $h \leq h_0$ and $X_{e^-} \leq X_{e^-,0}$. Take the pressure-affinity diagram for $s = 6.3$ kJ/kg-K, as an example (Fig. 4), the computed h and X_{e^-} show that only flows frozen at $p_f = 6.62$ atm or lower satisfy $X_{e^-} \leq X_{e^-,0}$ and the cutoff p_f between $h > h_0$ and $h < h_0$ is somewhere between 7–8 atm. For the argon nozzle flow considered here, it was found the requirement of $X_{e^-} \leq X_{e^-,0}$ was more restrictive than the requirement of $h < h_0$. Therefore, only the states that satisfy the requirement $X_{e^-} \leq X_{e^-,0}$ are included in the other figures. Linear pressure scale was utilized in Fig. 4 to show the details of the frozen flow curves of high p_f. F^* in the charts is the dimensional affinity F divided by the negative value of the heat of reaction at 0 K. That is,

$$F^* = F/H^0 \tag{29}$$

where

$$H^0 = -\sum \nu_j \Delta h_j \tag{30}$$

The computed temperature and pressure ranges for different flow cross-sectional areas are presented in Figs. 5 and 6 for s ranging from 6.213 ($=s_0$) to 7 kJ/kg-K. The valid states of argon plasma on a constant-entropy plane are bounded by the exit pressure, the LChE flow, and the frozen flow of the maximum possible p_f for the given s. At small A the difference between LChE and frozen flows is very small. As A increases, the region of valid states first increases, then decreases as the boundaries of $p = p_e$ and $F = 0$ approach each other, resulting in fewer valid states at large A.

Examination of the charts of different entropies shows that the range of valid plasma states decreases very rapidly as entropy increases. For $s = s_0$, frozen flow may occur anywhere between $p_f = p_0$ and p_e. But at $s = 7$ kJ/kg-K, only flows frozen at $p_f = 0.255$ atm or lower are possible. It was found that there was no valid state for argon plasma on the planes of $s = 7.35$ kJ/kg-K or higher. As a result, only nonequilibrium charts for $s = s_0$ to 7.35 kJ/kg-K are needed for the reservoir conditions of $T_0 = 15{,}000$ K and $p_0 = 10$ atm and an exit pressure of $p_e = 0.05$ atm.

The three-dimensional plot of p-A diagrams of different entropies resembles a leaning cone of triangular cross-section (see Fig. 5d). As entropy increases, not only the region of valid plasma states shrinks, but the projection of this region on the plane of $s = s_0$ begins to move out of the region of valid states at $s = s_0$. The T-A and F-A diagrams of different entropies (not shown due to space limit) behave in a similar manner. This observation explains why the state of a reacting flow may fall outside the bounds of the LChE and frozen flows calculated at $s = s_0$.

Since two of the three constraints on the valid plasma states, $p = p_e$ and $F = 0$, are plane surfaces in the three-dimensional coordinates of s, p, and F, it is more convenient to show the range of valid states of a reacting flow in terms of these three properties. The resultant plot of the plasma states is depicted in Fig. 7a. (It should be noted that Figs. 5d and 7a are conceptual sketches. The sides of the triangular cones are not all flat and the edges may not be straight.) Because the volume that envelops all the valid states forms a vertical triangular cone in Fig. 7a, the regions of valid states at high entropies should fall within the region of valid states at $s = s_0$. This is verified by the F-p diagrams shown in Figs. 7b–7d. In these affinity charts, the range of possible affinity values decreases with the frozen point pressure p_f. A flow frozen at a higher pressure releases less chemical energy, and therefore, has a higher F^* at the nozzle exit than the flow frozen at a lower pressure. Close examination of the p-F diagrams shows that the change in affinity is not sensitive to entropy change. For a given p_f, the frozen flow curves in the F-p diagrams of different s are almost identical. These observations suggest

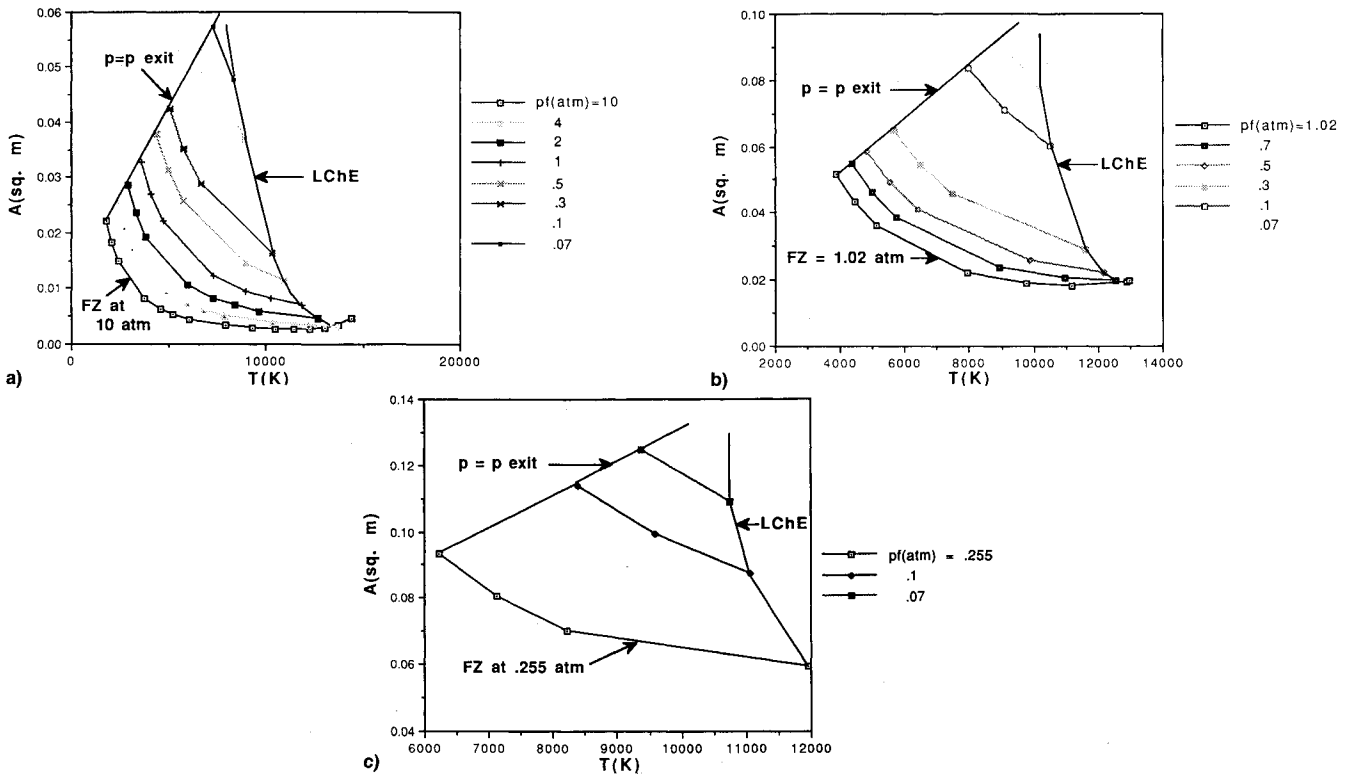

Fig. 6 Temperature-area diagrams of valid argon states at different entropies. s = a) 6.213 ($=s_0$), b) 6.7, and c) 7 kJ/kg-K.

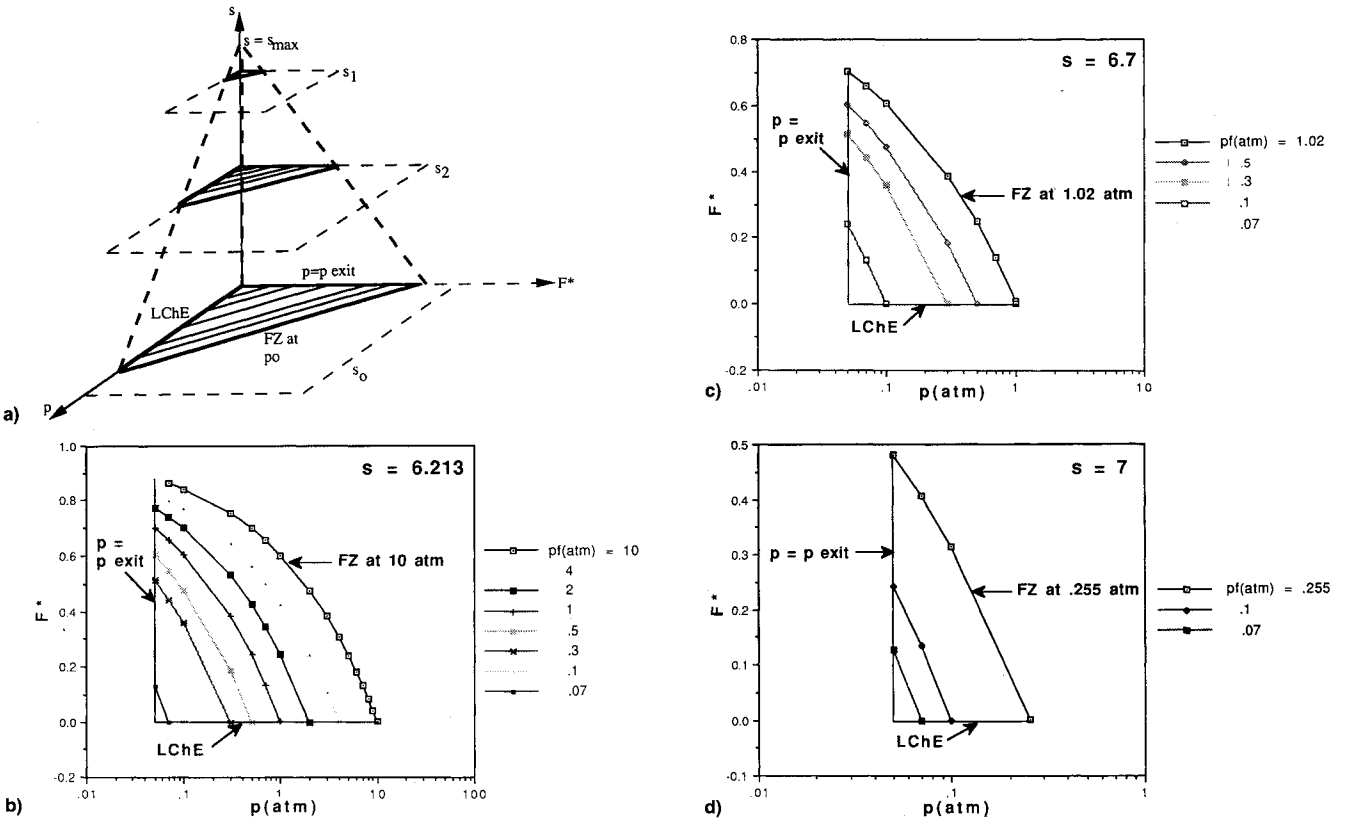

Fig. 7 Affinity-pressure diagrams of valid argon states at different entropies. s = a) 6.213–7, b) 6.213 ($=s_0$), c) 6.7, and d) 7 kJ/kg-K.

that the range of affinity variation in a reacting flow can be estimated from the LChE and frozen flows determined at $s = s_0$.

An example is given to illustrate the application of the nonequilibrium charts to a one-dimensional, inviscid flow of argon plasma in an adiabatic nozzle. If the argon plasma is discharged from 10 atm and 15,000 K and can be assumed to be in LChE from the inlet to the throat of the nozzle, variations of p, T, and A for unit mass flow rate in the convergent section of the nozzle can be determined from the LChE results in Figs. 5a and 6a for $s = s_0$. A and p at the nozzle throat are approximately 0.003 m^2 and 6 atm, respectively. The maximum F^* at the nozzle exit is expected to be less than 0.854 from Fig. 7b for $p_f = 6$ atm; if at a point downstream in the

divergent section of the nozzle, A, p, and T are measured to be 0.0222 m^2, 0.3 atm, and 8000 K, respectively. Inspection of the p-A and T-A diagrams of different entropies indicates that s and p_f at that point are 6.7 kJ/kg-K and 1 atm, respectively. Plasma velocity and F^* at this point are 3011 m/s and 0.383, respectively. If frozen flow can be assumed between this point and the nozzle exit, the plasma state will follow the frozen flow curve of $p_f = 1$ atm on the plane of $s = 6.7$ kJ/kg-K until the exit state is reached. At the nozzle exit F^* equals 0.7, which is within the range of F^* values estimated at $s = s_0$. Transition from LChE to frozen flow can be studied in detail and the complete process can be plotted on the nonequilibrium charts of different entropies if several T, p, and A measurements are made in the transition process. The end of transition is signaled by the near zero entropy increase in the reacting flow.

IV. Universal Affinity-Pressure Diagram

Figure 7a suggests that if the supersonic nozzle flow processes were plotted in three dimensions, then a view parallel to the altitude (s axis) of the right triangular cone would give a projection of each of the processes on a plane perpendicular to the s axis. It can be seen from Figs. 7b–7d that the projection of curves of a constant p_f from different entropy planes lie almost on top of each other (as shown in Fig. 8). These two statements enable the plotting of both equilibrium (LChE and frozen flow) and nonequilibrium processes on the one two-dimensional plot of affinity vs pressure.

Experimental work with plasma torches has shown that in the freejet obtained, the affinity (not the "flow") is frozen.[14,15] For pure argon, the dimensionless affinity value for atomic ionization is 25%.[15] Using data from the previous example, but setting $F^* = 0.25$ in the downstream part of the nozzle, one obtains the plot shown in Fig. 8. The S-shaped transition between the LChE and the frozen affinity flow has been furred in, keeping the first derivatives the same at the junctions. The exact shape is not known, but a good estimate is possible. Note that the frozen affinity process is much different than the frozen flow process. Part of the difference may be that the plasma torch freejet is at high pressure.

This example is given as being instructional only. At the high temperatures used here, the flow is actually viscous, not inviscid. Though it is expected that the affinity will be frozen over some of the divergent nozzle, there are a number of limitations: 1) the required experimental measurements have only been made in plasma free jets, 2) the volume over which measurements could be made is limited, and 3) the effect of multiple reactions is not known (e.g., hydrogen atomic ionization/recombination at high temperature followed by dissociative recombination at lower temperatures). The affinity may not be convenient to use if a large number of reactions are present, but then traditional methods are not convenient to use either.

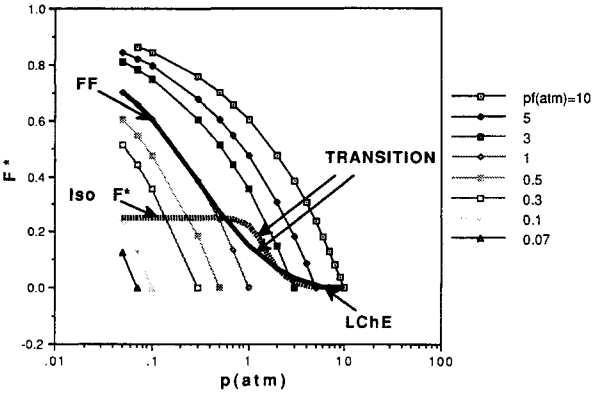

Fig. 8 Projections of p_f curves and conceptual plot of the supersonic nozzle flow processes: the LChE in the convergent nozzle, the furred in transition region in the throat, the frozen affinity process (Iso F^*) downstream in the divergent nozzle, and the alternative frozen flow process (FF) in the divergent nozzle; s = 6.213–6.7 kJ/kg-K.

V. Conclusions

A one-dimensional analysis was presented for developing nonequilibrium charts applicable to reacting flows. Argon plasma at 10 atm and 15,000 K discharged through an adiabatic, frictionless nozzle was investigated. The range of entropy variation was examined and discussed. Nonequilibrium charts of different entropies are needed for reacting flow analysis. The ranges of plasma properties at different entropies were plotted for different degrees of reaction extent and different degrees of irreversibility. At high entropies, the state of plasma flow at a given nozzle area may fall outside the bounds of the LChE and frozen flows determined at the reservoir entropy, but the affinity curves of frozen flows at different entropies show little entropy dependence. If plotted in terms of pressure, affinity, and entropy, the valid plasma states resemble a vertical cone of triangular cross section. The regions of valid plasma states at high entropies will fall within the valid state region at low entropies.

References

[1]Pierce, F. J., *Microscopic Thermodynamics*, International Textbook, Scranton, PA, 1968, pp. 364–367.

[2]Griem, H. R., *Plasma Spectroscopy*, McGraw–Hill, New York, 1964.

[3]Phelps, A. V., "Cross Sections and Swamp Coefficients for H^+,H_2^+,H_3^+,H, H_2, and H^- in H_2 for Energies from 0.1 eV to 10 kev," *Journal of Physical and Chemical Reference Data*, Vol. 19, No. 3, 1990, pp. 653–675.

[4]Lelevkin, V. M., Otorbaev, D. K., and Schram, D. C., *Physics of Non-Equilibrium Plasmas*, North-Holland, Amsterdam, 1992, pp. 313–409.

[5]Anderson, J. D., *Modern Compressible Flow*, McGraw–Hill, New York, 1982, pp. 403–434.

[6]Sutton, G. P., *Rocket Propulsion Elements*, 5th ed., Wiley, New York, 1986, pp. 131–144.

[7]De Donder, Th., and Van Rysselberghe, P., *Thermodynamic Theory of Affinity*, Stanford Univ. Press, Stanford, CA, 1936, p. 34.

[8]Haase, R., *Thermodynamics of Irreversible Processes*, Addison–Wesley, Reading, MA, 1969, p. 39.

[9]Chen, K., and Eddy, T. L., "Composition and Partition Functions of Partially Ionized Hydrogen Plasma in Non-Local Thermal Equilibrium and Non-Local Chemical Equilibrium," *Journal of Non-equilibrium Thermodynamics*, Vol. 18, No. 1, 1993, pp. 1–18.

[10]Chen, K., and Eddy, T. L., "Thermodynamic Properties of Molecular Hydrogen Plasma in Thermal and Chemical Nonequilibrium," *Journal of Thermophysics and Heat Transfer*, Vol. 7, No. 2, 1993, pp. 277–284.

[11]Sonntag, R. E., and Van Wylen, G. J., *Fundamentals of Statistical Thermodynamics*, Wiley, New York, 1966, pp. 262, 263.

[12]Sedghinasab, A., and Eddy, T. L., "Nonequilibrium Thermodynamic Properties of Argon," *Heat Transfer in Thermal Plasma Processing*, American Society of Mechanical Engineers, HTD-Vol. 161, New York, 1991, pp. 187–193.

[13]Chen, K., and Eddy, T. L., "Investigation of Chemical Affinity for Reacting Flows of Non-LThE Gases," AIAA Paper 93-3225, July 1993.

[14]Eddy, T. L., Detering, B. A., and Wilson, G. C., "LTE and Non-LTE Temperatures in Loaded and Unloaded Plasmas During Spraying of NiAl Powders," *Thermal Spray Research and Applications*, ASM International, Materials Park, OH, 1991, pp. 33–37.

[15]Eddy, T. L., Grandy, J. D., and Detering, B. A., "Chemical Nonequilibrium in an Argon Plasma Torch Plume," *Heat Transfer in Thermal Plasma Processing*, American Society of Mechanical Engineers, HTD-Vol. 161, New York, 1991, pp. 79–88.